metals

MDPI

Article

# A Study on Cutting Force of Machining In Situ $TiB_2$ Particle-Reinforced 7050Al Alloy Matrix Composites

**Yifeng Xiong †, Wenhu Wang †, Ruisong Jiang * and Kunyang Lin**

The Key Laboratory of Contemporary Design and Integrated Manufacturing Technology, Ministry of Education, Northwestern Polytechnical University, Xi'an 710072, Shaanxi, China; xiongyifeng@mail.nwpu.edu.cn (Y.X.); npuwwh@nwpu.edu.cn (W.W.); linkunyang@mail.nwpu.edu.cn (K.L.)

* Correspondence: jiangrs@nwpu.edu.cn; Tel.: +86-15029225233

† These authors contributed equally to this work.

Academic Editor: Andrew Kennedy

Received: 22 February 2017; Accepted: 24 May 2017; Published: 27 May 2017

**Abstract:** In situ $TiB_2$ particle-reinforced 7050Al alloy matrix composites are a new category of particulate metal matrix composites with improved mechanical and physical properties. At present, the study of machining in situ $TiB_2$/Al composite is limited and no specific study has been presented on cutting force. Based on previous work, experimental investigation of cutting in situ $TiB_2$/Al composite was carried out in this study to investigate the cutting force, shear angle, mean friction angle, and shear stress. The results indicated that the feed rate, instead of cutting speed, has a significant influence on the shear angle, mean friction angle, shear stress, and forces, which is different from cutting ex situ SiC/Al composites. Meanwhile, based on Merchant's theory, a force model, which consists of chip formation and ploughing force, was established to have a better understanding of force generation. A comparison of the results show an acceptable agreement between the force model and experiments. Additionally, at varying feed rates, the linear relationship between the shear angle and mean friction angle is still suitable for cutting in situ $TiB_2$/7050Al alloy composites.

**Keywords:** in situ; metal-matrix composites (MMCs); $TiB_2$ particles; Al; cutting force; modeling

## 1. Introduction

Particle-reinforced metal matrix composites (PRMMCs) play an important role in modern industry and tend to replace conventional metal materials due to their superior mechanical and physical properties, such as improved strength, low density and cost, perfect low-temperature performance, and increased wear resistance [1]. According to particle forming methods, PRMMCs are classified into two categories: ex situ and in situ PRMMCs.

Since the 1970s, many machining studies, such as cutting, grinding, wire-electrode cutting, and laser assisted machining [2–7], have been carried out on ex situ PRMMCs, whose preparation technology is simple, especially ex situ SiC particle-reinforced aluminum matrix composite. It is found from many studies that, with hard ceramic particles (e.g., SiC, $TiB_2$, $Al_2O_3$), the tool wear is terrible and the cutting force is large, which makes machining PRMMCs complex. In order to have a deep insight into the cutting mechanism of PRMMCs, a large number of studies have been carried out on cutting force and force modeling.

Jenarthanan and Krishnamurthy investigated the metal removal rate of machining in situ $TiB_2$/Al composites, respectively [8,9]. They both concluded that cutting speed and feed have a dominant effect on material removal rate. Additionally, with scanning electron microscope (SEM) images, Jenarthanan found that the distribution of $TiB_2$ particles was more or less homogenous. Mahamani and Anandakrishnan researched the influence of cutting parameters and the reinforcement ratio on tool

wear, force, and surface roughness with Al-5Cu-$TiB_2$ in situ PRMMs and Al-6061-$TiB_2$ in situ PRMMCs, respectively [10,11]. From experimental results, they both found that there would be an increase in flank wear, force, and roughness as the feed rate increased. Recently, in our previous study of machining in situ $TiB_2$/7050Al composites [12–14], the surface integrity, such as surface roughness, residual stress, and microhardness, and tool wear mechanisms were studied. From the SEM images of machined workpiece surface and EDS (energy dispersive spectrometry) of the worn tool face, it was found that no particle pull-out or fracture phenomena occurred, which was different from machining SiC/Al composites [15–17].

However, in the machining performance study of a new kind of material, simple experimental study is not enough. Analytical force modeling is needed to investigate the material removal mechanism. Until now, there has been no analytical force modeling report for in situ PRMMCs published, while most of the force modeling work was focused on ex situ SiC/Al composites.

In 2004, Kishawy [18] proposed an analytical force model for cutting SiC/Al composites based on the energy method. It could predict cutting force successfully under the following assumptions: (a) energy in the first deformation zone is three times that in the secondary deformation zone, which is a result from steel machining experiments; and (b) the initial and final particle crack lengths are assumed to be 1 μm with no justification.

Later in 2006, based on Merchant's analysis [19], Davim et al. and Pramanik et al. developed analytical force model with PCD (polycrystal diamond) tools, respectively [20,21]. In Davim's model, the ex situ SiC/Al composite was treated as an equivalent homogenous material without justification. However, based on the discovery of particle fracture and displacement during the cutting process [22–24], Pramanik et al. thought the effect of particles on force generation could not be ignored. Then, in their model, the cutting force was decomposed into chip formation force, ploughing force, and particle fracture force. Based on Merchant's theory, the slip-line field theory, and the Griffith theory, the cutting force model was established. The chip deformation was assumed to occur only in the shear plane, while the chip-tool interface friction force due to the hard particles was out of consideration.

In 2009, Dabade et al. [25] developed a model of chip-tool friction in orthogonal cutting ex situ SiC/Al composite with PCD tools. However, in this model, both the effect of the ploughing force produced by the tool cutting edge and the particle fracture force due to hard particles were ignored. Sikder and Kishawy proposed a modified model based on Pramanik's model in 2012 [26]. Different from Pramanik's force model, the Johnson-Cook (J-C) constitutive model was used in calculating the chip deformation force. An assumption was made that the particles were spherical. Additionally, two-body and three-body rolling friction theory were applied in obtaining the chip-tool friction force.

Compared with ex situ $SiC_p$/Al MMCs (metal-matrix composites), the in situ $TiB_2$ particle-reinforced 7050Al alloy composites have evenly-distributed and smaller particles. Additionally, the particle-matrix interface is clean and no obvious particle pull-out phenomenon has been found in our previous cutting study, which is different from that of cutting ex situ $SiC_p$/Al MMCs. In order to have a better understanding of cutting this new kind of in situ PRMMC, the cutting force of machining in situ $TiB_2$ particle-reinforced 7050Al alloy composite was researched and an attempt was made to build a force model based on the shear plane theory. Furthermore, with the experimental results of cutting forces and chip thickness, the shear angle, mean friction angle, and shear stress were also investigated.

## 2. Materials and Methods

### *2.1. Tool and Workpiece Material*

PCD straight cutting edge mills were used in tests. The tool diameter is 12 mm and the rank and flank angles were 8° and 10°, respectively. Each mill has two straight cutting edges with an edge radius of 0.02 mm. The chemical composition of the 7050Al alloy matrix, particle size, and volume are shown in Tables 1 and 2. The workpiece material, whose microstructure is presented in Figure 1, was in situ 6 wt % $TiB_2$/7050Al composites prepared by an exothermic reaction process [27] at Shanghai

Jiao Tong University. The main exothermic reaction process during the material preparation process is as follows:

$$\begin{gathered} 2KBF_4 + 3Al = AlB_2 + 2KAlF_4 \\ AlB_2 + TiAl_3 = TiB_2 + 4Al \end{gathered} \quad (1)$$

**Table 1.** Chemical composition of the matrix material.

| Elements | Zn | Zr | Mg | Cu | Al |
|---|---|---|---|---|---|
| Composition (wt %) | 6.3 | 0.11 | 2.3 | 2.2 | Balanced |

**Table 2.** Size and volume of particles.

| Particle | Size | Volume |
|---|---|---|
| $TiB_2$ | 50–200 nm | 6% |

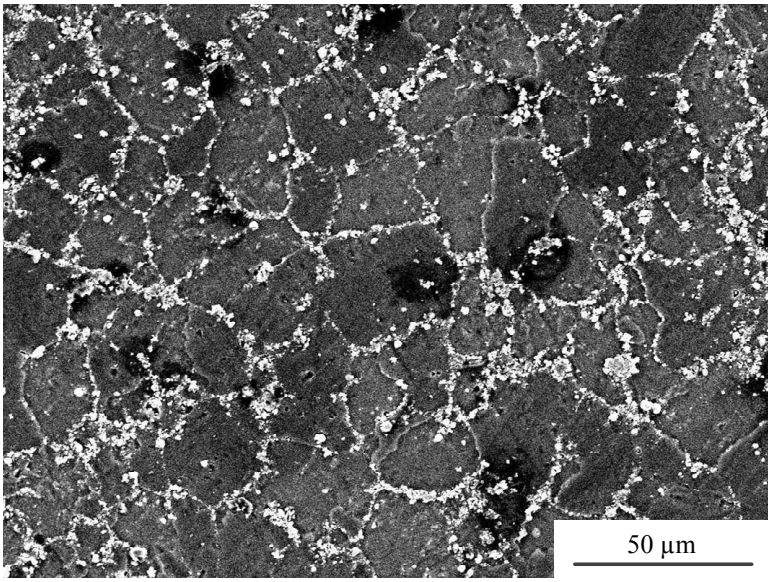


**Figure 1.** Microstructure of the composite used in the experiments.

## 2.2. Experiment Design

The down-milling experiments were carried out under dry conditions. A computer numerical control milling machine (type YHVT850Z, Yonghua Machinery Co. Ltd., Yanzhou, China), whose spindle power is 5.5 kW and maximum spindle speed is 8000 rpm, was applied in our study. For orthogonal cutting with straight cutting edge mills, the workpieces were cut into sheets, as shown in Figure 2. Table 3 shows the detailed parameter levels during tests.

**Table 3.** Detailed parameter levels for single-factor tests.

| Factors | Notation | Level | | | | | |
|---|---|---|---|---|---|---|---|
| | | 1 | 2 | 3 | 4 | 5 | 6 |
| Cutting speed (m/min) | $v_c$ | 20 | 30 | 40 | 50 | 60 | 70 |
| Feed rate (mm/z) | $f_z$ | 0.1 | 0.2 | 0.3 | 0.4 | 0.5 | 0.6 |
| Cutting depth (mm) | $a_p$ | 1 | 2 | 3 | 4 | | |
| Cutting width (mm) | $a_e$ | 8 | | | | | |

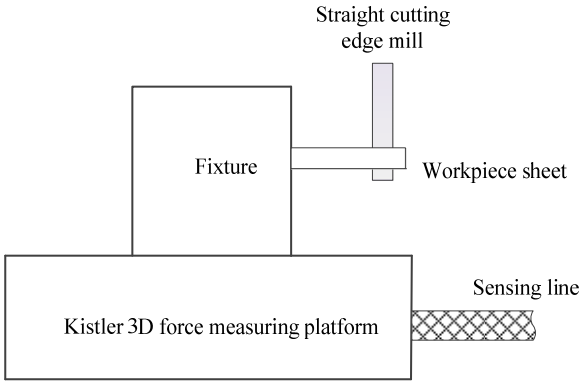


**Figure 2.** Experimental design and process.

During the experiments, a Kistler 3D force measuring platform (type 9255B, Kistler, Winterthur, Switzerland) was used to measure cutting forces. For each experiment, cutting was performed for over 15 s and repeated three times. After each test, chips were collected and a micrometer was used to measure the chip thickness five times and the average value was selected for calculating the shear angle.

## 3. Effect of Cutting Parameters

In the actual milling process, the directions of instantaneous cutting forces $F_c$ (force in the cutting direction) and $F_t$ (force in the feed direction) change every moment, as shown in Figure 3a. However, the directions of measured cutting forces $F_x$ and $F_y$ are invariable as the Kistler force measuring platform settled. Hence, a transformation from measured cutting forces to instantaneous cutting forces is needed with a given immersion angle $\theta$, presented in Figure 3a by Equation (2):

$$\begin{bmatrix} F_c \\ F_t \end{bmatrix} = \begin{bmatrix} \sin\theta & \cos\theta \\ -\cos\theta & \sin\theta \end{bmatrix} \begin{bmatrix} F_x \\ F_y \end{bmatrix} \quad (2)$$

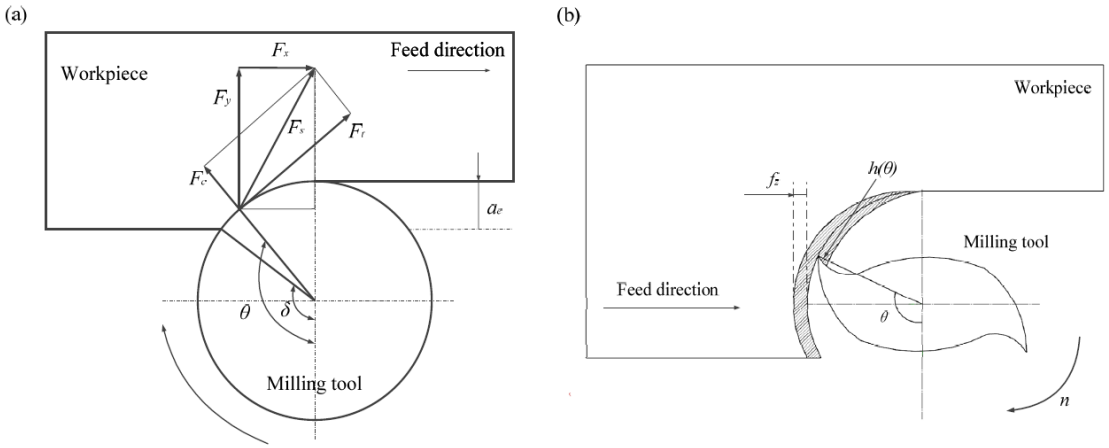


**Figure 3.** Peripheral milling process with straight cutting edges: (**a**) directions of instantaneous cutting forces; (**b**) uncut chip thickness.

However, during down-milling experiments with straight cutting edges mills, the uncut chip thickness and cutting forces both change with the immersion angle $\theta$, as shown in Figure 3b. As the maximum chip thickness was measured and considered in the following force modeling, the cutting forces should be calculated as follow:

$$\begin{bmatrix} F_c \\ F_t \end{bmatrix} = \begin{bmatrix} \sin\delta & \cos\delta \\ -\cos\delta & \sin\delta \end{bmatrix} \begin{bmatrix} F_x \\ F_y \end{bmatrix} \tag{3}$$

where $\delta$ is the immersion angle at the maximum uncut chip thickness under a certain cutting width $a_e$, which could be determined using Equation (4):

$$\delta = \begin{cases} \frac{\pi}{2} + \sin^{-1}\frac{D/2-a_e}{D/2} & (a_e \leq D/2) \\ \frac{\pi}{2} & (a_e > D/2) \end{cases} \tag{4}$$

With Equations (3) and (4), the instantaneous cutting forces could be obtained using measured cutting forces. The effect of cutting parameters on cutting forces is shown in Figure 4. It can be seen that the force in the feed direction is larger than that along the cutting direction. Additionally, the different values between the forces in feed and cutting directions changes little with an increase in the cutting speed, except at 30 m/min. However, it tends to get larger as the feed rate or cutting depth increases.

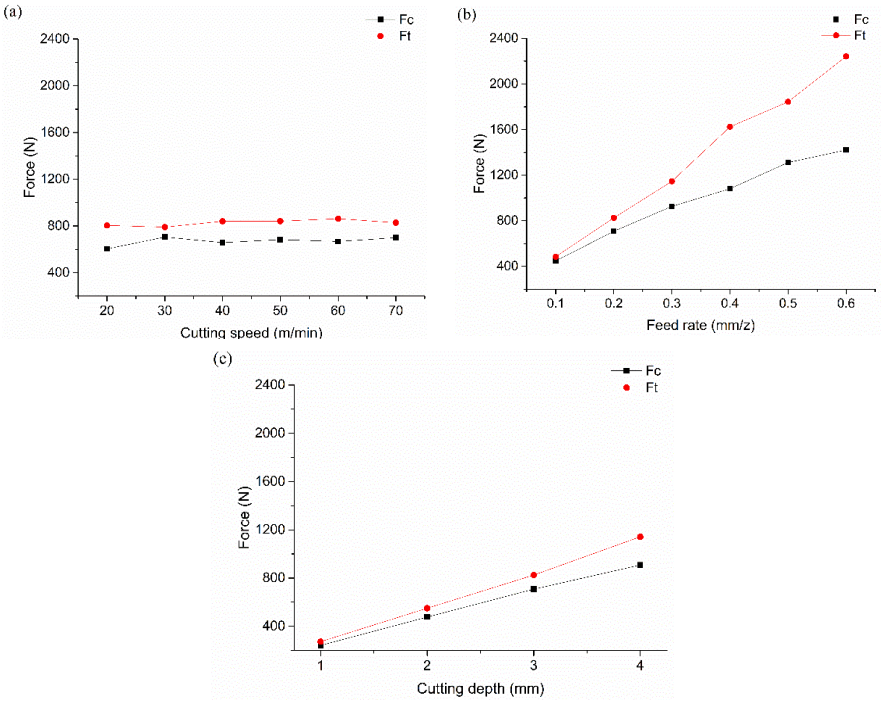


**Figure 4.** Effect of cutting parameters on forces: (**a**) $f_z$ = 0.2 mm/z, $a_p$ = 3 mm; (**b**) $v_c$ = 40 m/min, $a_p$ = 3 mm; and (**c**) $v_c$ = 40 m/min, $f_z$ = 0.2 mm/z.

Meanwhile, it is obvious that the feed rate has the highest influence on cutting forces followed by cutting depth and speed. With an increase in the feed rate or cutting depth, the cutting forces increase linearly. This may be due to the increase of the cutting area and removed material volume as the feed rate or cutting depth increased. Additionally, in low-speed cutting (the spindle speed is around 1857 r/min as the cutting speed equals 70 m/min), the cutting speed does not significantly influence the cutting forces, as shown in Figure 4a. The presence of hard particles resulted in the highly brittle nature of in situ $TiB_2$/7050Al composites, which can be seen from the common formed saw-teeth chips at low cutting speed, as shown in Figure 5. Thus, with using PCD tools, the friction at the chip-tool interface was small, resulting in little fluctuation of the cutting force as the cutting speed increased.

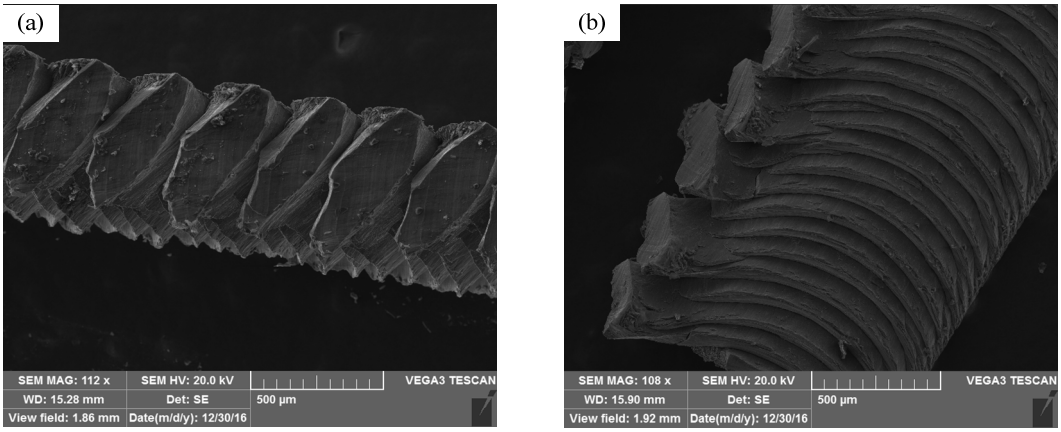


**Figure 5.** Common formed saw-teeth chips under low cutting speed: (**a**) side face of saw-teeth chip; and (**b**) free surface of saw-teeth chip.

In most cases during low speed cutting, cutting speed does not influence the cutting forces significantly. However, according to studies and discoveries of machining ex situ SiC/Al composites [28,29], some contradictory reports were found. With the presence of the BUE (built-up edge), forces at low cutting speeds are lower than that at high speeds. However, what is different from machining ex situ $SiC_p$/Al composites is that there is no obvious decrease or increase in the cutting forces as the cutting speed increases. To have a better understanding of the cutting force in machining in situ $TiB_2$/7050Al composites, the work of force modeling is needed and will be discussed in the following section.

## 4. Modeling of Machining Forces

With the in situ synthesis method, the in situ $TiB_2$/Al composite obtains a much better adhesion at interfaces between ceramic particles and matrix material. Compared with the preparation method and process of ex situ PMMCs, the reinforcement is generated in matrix material through chemical reactions during the whole material preparation process. Additionally, in our previous studies, no particle pull-out or fracture phenomena have been found.

Given all of this, it can be seen that the in situ $TiB_2$/Al composite could not be treated as a simple combination of particles and matrix material. Considering the small size and volume of particles (size: 50–200 nm, volume: 6 wt %) and high viscosity of the matrix material, it is assumed that the in situ $TiB_2$/Al composite is an equivalent homogenous material, which means that the particle fracture force is no longer treated separately. Hence, the cutting force consists of two main parts: (a) chip formation force; and (b) ploughing force. Then the analytical force model can be expressed as follows:

$$\begin{aligned} F_c &= F_{cc} + F_{cp} \\ F_t &= F_{tc} + F_{tp} \end{aligned} \tag{5}$$

where $F_c$ represents the resultant force in cutting direction, and $F_t$ represents the resultant force in thrust direction. $F_{cc}$ and $F_{cp}$ stand for the chip formation and ploughing forces along the cutting direction, respectively. $F_{tc}$ and $F_{tp}$ represent the chip formation and ploughing forces in the thrust direction, respectively.

### *4.1. Computing Shear Angle, Mean Friction Angle, and Shear Stress*

In order to calculate the cutting forces $F_{cc}$ and $F_{tc}$, the shear angle $\phi$, mean friction angle $\beta$, and shear stress $\tau_s$ are needed. In milling processes, the true tooth path is a composition of the rotary motion of the tool with the rectilinear motion of the workpiece along the feed direction. Hence, the actual tooth path shape of a cutter during milling process is a trochoid, which is also named an

elongated cycloid, as shown in Figure 6. However, as the feed rate $f_z$ is much smaller than the cutter diameter $D$, a circular tool-path approximation is mostly used by neglecting the actual trochoidal tool motion [30].

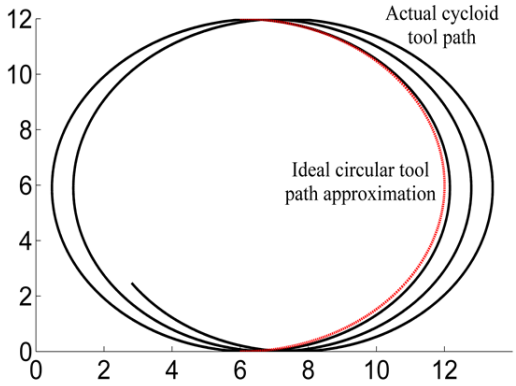


**Figure 6.** The actual cycloid tool path of a milling cutter and the widely-used ideal circular tool-path approximation.

With this assumption, the uncut chip thickness, which is defined as $h$ in Figure 7, $h(\theta)$ in Figure 3b could be calculated easily. Then the maximum uncut chip thickness $h_{max}$ could also be determined with Equations (4) and (6):

$$\begin{array}{c} h(\theta) = f_z \cdot \sin\theta \\ h_{max} = max\{h(\theta)\} \end{array} \quad \theta \in [\delta, \pi] \tag{6}$$

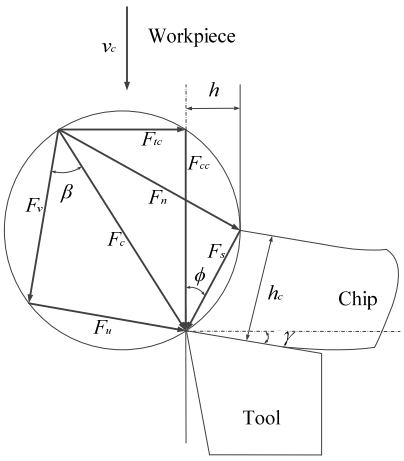


**Figure 7.** Merchant's orthogonal cutting model.

Then, based on the shear plane theory, the shear angle here could be determined from the chip compression ratio as follows:

$$\tan\varnothing = \frac{R_c \cdot \cos\gamma}{1 - R_c \cdot \sin\gamma} \tag{7}$$

where $\gamma$ represents the tool rank angle and $R_c$ is the chip compression ratio. The chip compression ratio could be calculated with the measured chip thickness after cutting tests as below:

$$R_c = \frac{h_c}{h_{max}} \tag{8}$$

where $h_c$ and $h_{max}$ represent the measured chip thickness and the maximum uncut chip thickness, respectively.

Meanwhile, with the cutting forces measured in Section 3, the mean friction angle $\beta$ could also be calculated with Equations (3) and (4) and the following Equation (9):

$$\tan(\beta - \gamma) = \frac{F_{tc}}{F_{cc}} \tag{9}$$

In some studies, the shear stress was treated as a constant parameter. However, shear stress is different and fluctuates in a definitive range under different cutting parameters. In order to obtain exact shear stress, it will be determined experimentally in this study. With measured forces $F_x$ and $F_y$, the cutting and thrust forces could be determined with Equations (3) and (4). Then the shear stress on the shear plane could be determined using the following equation:

$$\tau_s = \frac{F_c \cos \varnothing - F_t \sin \varnothing}{A/\sin \varnothing} \tag{10}$$

where $A$ is the cross-sectional area of the cut.

The shear angle $\phi$ is the angle at which the shearing phenomenon occurs, as the shear stress reaches the material shear strength. In analytical cutting force modeling, the shear angle $\phi$ is one of the most important factors which has great influence on chip shape and cutting forces, whether using the shear plane method or using the shear zone method. According to Pramanik [30], at varying cutting speeds, the linear relationship between shear angle $\phi$ and $(\beta - \gamma)$, which was observed in machining monolithic metal, is still approximately suitable for cutting ex situ SiC/Al composites, as shown in Equation (11):

$$\varnothing = \frac{\pi}{5} - \frac{1}{2}(\beta - \gamma) \tag{11}$$

However, whether the relationship in Equation (11) is still suitable for cutting in situ $TiB_2$/7050Al composites is unknown and needs further study. During orthogonal cutting of in situ $TiB_2$/Al composites, as discussed in Section 3, it is obvious that the feed rate plays an important role on cutting forces. Then the relationship between shear angle $\phi$ and $(\beta - \gamma)$ at varying feed rate is shown in Figure 8.

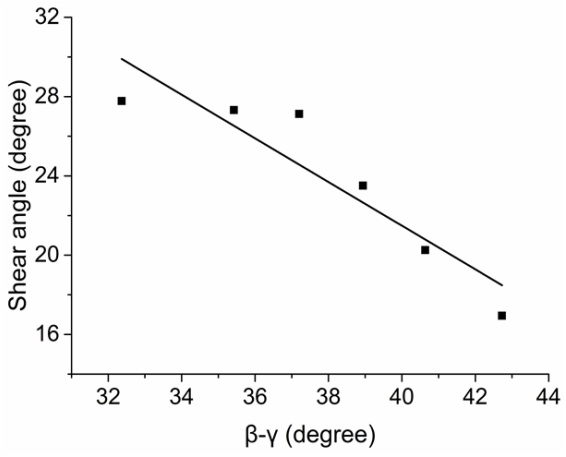


**Figure 8.** Relationship between $(\beta - \gamma)$ and shear angle $\phi$ at varying feed rates.

From Figure 8, it is obvious that the linear relationship is still suitable for cutting in situ $TiB_2$/Al composites at varying feed rates and it is given with the following linear regression:

$$\varnothing = \frac{\pi}{3} - 1.1(\beta - \gamma) \tag{12}$$

Then the relationship between the feed rate and shear angle, mean friction angle, and shear stress could be determined, as follows:

$$\begin{cases} \varnothing = 15.92 + 22.57 f_z\,, & R = 0.901 \\ \beta = 52.80 - 19.76 f_z\,, & R = 0.989 \\ \tau_s = 355.9 - 369.1 f_z + 575.9 f_z^2\,, & R = 0.956 \end{cases} \tag{13}$$

Thus, the shear angle $\phi$, mean friction angle $\beta$ and shear stress $\tau_s$ for calculating the chip formation force could be determined using Equation (13).

### *4.2. Chip Formation and Ploughing Forces*

The single shear plane model from Merchant is applied in this study for the chip formation force. With the shear angle $\phi$, mean friction angle $\beta$, and shear stress $\tau_s$ calculated in Section 4.1, the chip formation forces in cutting and feed directions can be calculated with the following equations:

$$\begin{aligned} F_{cc} &= \tau_s A \frac{\cos(\beta-\gamma)}{\sin\varnothing\cos(\varnothing+\beta-\gamma)} \\ F_{tc} &= \tau_s A \frac{\sin(\beta-\gamma)}{\sin\varnothing\cos(\varnothing+\beta-\gamma)} \end{aligned} \tag{14}$$

where $A$ is the cross-sectional area of the cut, and $\gamma$ is the tool rank angle, respectively.

Meanwhile, the matrix metal Al is easier to be softened under high cutting temperature, which makes it easier to adhere to the cutter edge. The ploughing force produced by the cutter edge should be considered in force modeling. Since the in situ $TiB_2$/Al composite is treated as an equivalent homogenous material and the particle size and volume are too small (size: 50–200 nm; volume: 6 wt %), only the matrix material Al is assumed to take part in ploughing.

Based on the slip line field method, the ploughing forces, such as $F_{cp}$ in the cutting direction and $F_{tp}$ along the feed direction, could be determined by considering the edge radius $r_n$ [31]:

$$\begin{aligned} F_{cp} &= \tau_m l r_n \tan\left(\tfrac{\pi}{4} + \tfrac{\gamma}{2}\right) \\ F_{tp} &= \tau_m l r_n \left[1 + \tfrac{\pi}{2}\right] \tan\left(\tfrac{\pi}{4} + \tfrac{\gamma}{2}\right) \end{aligned} \tag{15}$$

where $\tau_m$ is the shear stress of the matrix material and $l$ represents the active cutting edge length.

## 5. Verification and Results

To validate the force model in Section 4, a group of tests was carried out. The predicted chip formation force was calculated with Equations (13) and (14) and the ploughing force was determined by Equation (15). Then, using Equation (5), the resultant forces in cutting and thrust directions could be obtained.

Figure 9 shows the comparison results between predicted and measured forces under varying cutting depths. It is obvious that the cutting forces increase as the cutting depth increases, and that the increasing rate of cutting force is slightly larger than that of the thrust force under different cutting depths. Additionally, the predicted force results of analytical force model show a same trend with measured forces with an error of less than 9%, which shows an excellent quantitative agreement with the analytical force model developed before.

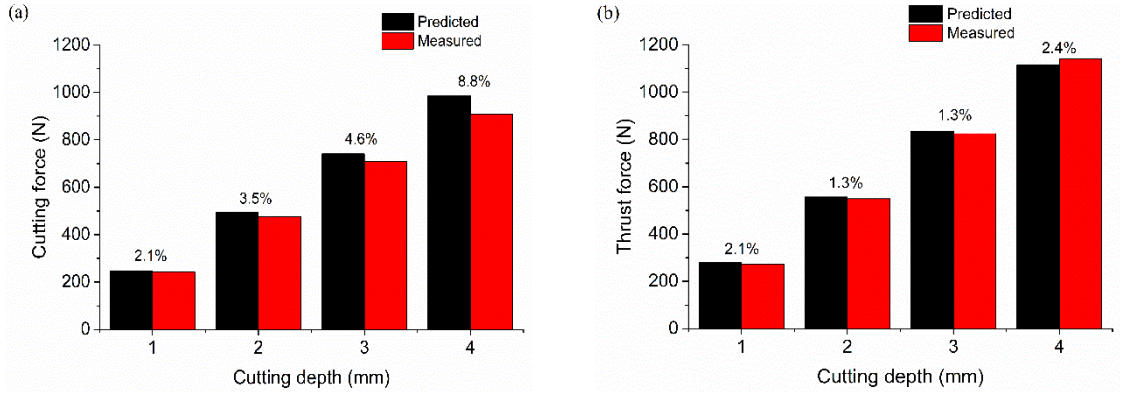


**Figure 9.** Comparison between the predicted and measured forces at varying cutting depth ($v_c$ = 40 m/min, $f_z$ = 0.2 mm/z): (**a**) cutting force; and (**b**) thrust force.

Figure 10 shows a comparison between the predicted and measured forces at different feed rates. As analyzed before, the feed rate has a dominant influence on cutting forces and, from Figure 10a,b, it can be seen that whether the predicted cutting and thrust forces or the measured ones all increase linearly as the feed rate increases, which verifies the conclusion made before.

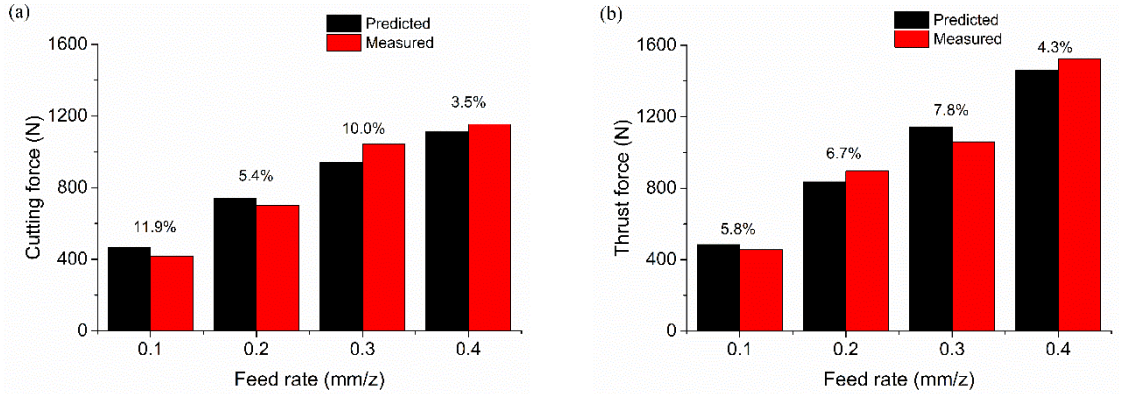


**Figure 10.** Comparison between the predicted and measured forces at varying feed rate ($v_c$ = 40 m/min, $a_p$ = 3 mm): (**a**) cutting force; and (**b**) thrust force.

Finally, four groups for comparison with varying combinations of cutting parameters were performed with a prediction error within 9%, as shown in Figure 11. Moreover, the effect of the cutting speed on the predicted and measured cutting forces is so small that it could be ignored, which is accordant with the conclusion that the cutting speed has a minimal influence on the cutting force, shear angle, and shear stress, as discussed in Sections 3 and 4. With large feed and depth, as shown in group #2, the predicted and measured forces are both the largest. With small feed and depth, as group #1 or #3, the forces predicted and measured both decrease.

From the 12 groups of verification test results shown in Figures 9–11, the average prediction error is 9%, indicating that it is acceptable for the force model developed in Section 4. From the test results, the conclusions made about influence of the feed rate and cutting speed on the shear angle, mean friction angle, shear stress, and cutting forces before are also acceptable.

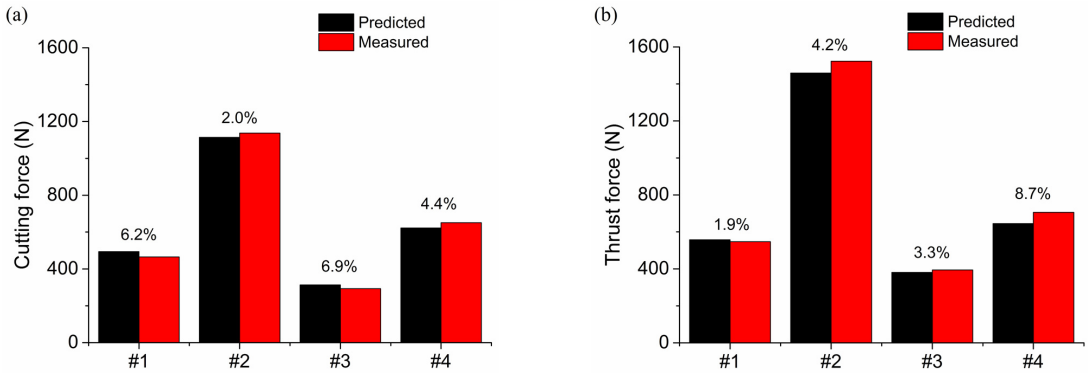


**Figure 11.** Comparison between the predicted and measured forces under different combination of cutting parameters: (**a**) cutting force; and (**b**) thrust force; (#1) $v_c$ = 20 m/min, $f_z$ = 0.2 mm/z, $a_p$ = 2 mm; (#2) $v_c$ = 30 m/min, $f_z$ = 0.4 mm/z, $a_p$ = 3 mm; (#3) $v_c$ = 40 m/min, $f_z$ = 0.3 mm/z, $a_p$ = 1 mm; (#4) $v_c$ = 50 m/min, $f_z$ = 0.1 mm/z, $a_p$ = 4 mm.

Additionally, the shear angle and mean friction angle were also investigated in this study. Figure 12 shows the influence of cutting parameters on shear and mean friction angles during cutting in situ $TiB_2$/Al composites. For the shear angle, from Figure 12a,c, it seems that the cutting speed and cutting depth do not significantly influence the shear angle. With the cutting speed or depth increasing, the shear angle increases and decreases slightly, respectively. However, it increases linearly as the feed rate increases from 0.1 mm/z to 0.4 mm/z, and the shear angle increases slightly when the feed rate exceeds 0.4 mm/z, as presented in Figure 12b. Furthermore, from Figure 12, it is obvious that the feed rate influences the shear angle significantly, which is the same as the effect on cutting forces in Section 3.

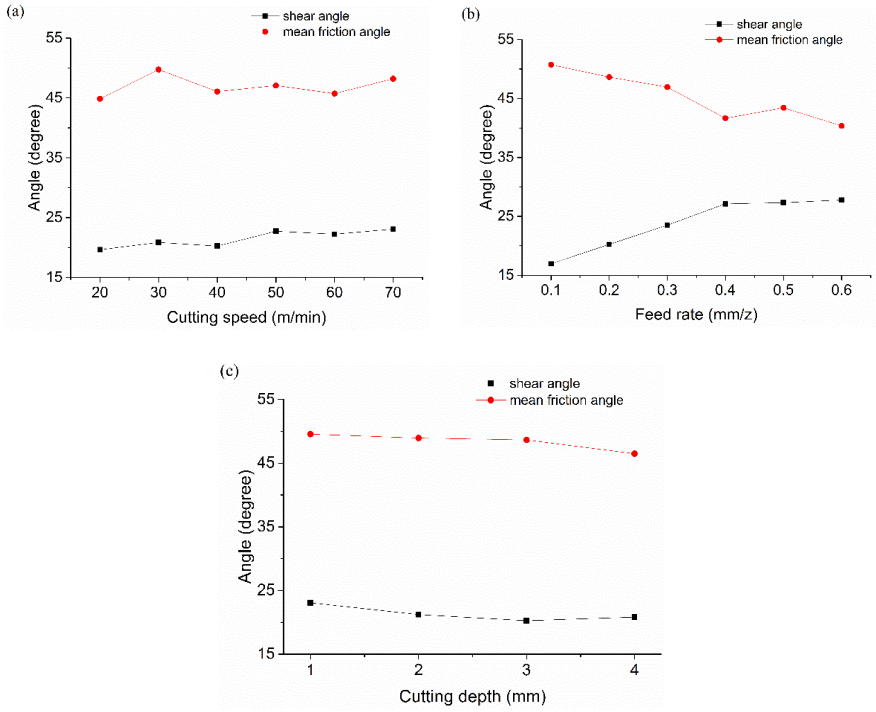


**Figure 12.** Effect of cutting parameters on shear and mean friction angle: (**a**) cutting speed; (**b**) feed rate; and (**c**) cutting depth.

Regarding the mean friction angle, the same phenomenon is also found in Figure 12a–c that the feed rate also has a dominant influence on the mean friction angle. In Figure 12c, with the increasing cutting depth, the mean friction angle decreases slightly. However, as the cutting speed increases, the mean friction angle fluctuates slightly around 48 degrees, and no obvious increase or decrease was found under the considered cutting speed.

## 6. Conclusions

In this study, the force, shear angle, mean friction angle, shear stress, and normal stress were researched in cutting in situ $TiB_2$/7050Al alloy composite. Additionally, with Merchant's theory, a force model was proposed for cutting force prediction. Based on the experimental results of orthogonal cutting tests with two straight cutting edges, the following conclusions can be drawn:

1. With the in situ synthesis method, the in situ TiB2/Al composite was treated as an equivalent homogenous material. The cutting force was considered to consist of chip formation and ploughing forces, which were calculated based on the single shear plane method and the slip line field theory, respectively. Additionally, comparison tests showed an excellent and acceptable agreement between the predicted forces and the experimental ones.
2. On the contrary of cutting ex situ SiCp/Al MMCs, it was found that, at varying feed rates instead of cutting speeds, the linear relationship between the shear angle $\phi$ and $(\beta - \gamma)$ seems to be still suitable for cutting in situ TiB2/7050Al composites:

$$\varnothing = \frac{\pi}{3} - 1.1(\beta - \gamma)$$

3. It seems that the influence of cutting parameters on normal stress is higher than that on shear stress. Similarly with ex situ SiC/Al MMCs, the normal stress of cutting in situ $TiB_2$/Al composites increases with an increase in the cutting speed. Differently, the normal stress also increases as the feed rate increases, which is opposite to ex situ SiC/Al MMCs. However, the shear stress seems to fluctuate slightly around 300 MPa under different cutting parameters.
4. Among all of the cutting parameters, feed rate plays an important role in the cutting forces, shear angle, mean friction angle, shear stress, and normal stress, instead of the cutting speed, which is found to have a dominant influence on measured forces $F_{cc}$, $F_{ct}$, and shear angle $\phi$ in cutting ex situ SiC/Al composites. The relationship between the feed rate and shear angle, mean friction angle, and shear stress is given below:

$$\begin{cases} \varnothing = 15.92 + 22.57 f_z \\ \beta = 52.80 - 19.76 f_z \\ \tau = 355.9 - 369.1 f_z + 575.9 f_z^2 \end{cases} \quad (16)$$

**Acknowledgments:** The authors would like to thank Dong Chen from Shanghai Jiao Tong University for his help in the experiments. Additionally, this work is sponsored by Innovation Foundation for Doctor Dissertation of Northwestern Polytechnical University (grant No. CX201613), National Natural Science Foundation of China (grant Nos. 51475374, 51505387), and Fundamental Research Funds for the Central Universities (grant No. 3102015ZY087).

**Author Contributions:** Yifeng Xiong, Wenhu Wang, and Ruisong Jiang conceived and designed the research; Yifeng Xiong and Kunyang Lin performed the experiments and analyzed the data; Yifeng Xiong wrote the paper; and Wenhu Wang and Ruisong Jiang contributed to writing and editing of the paper.

**Conflicts of Interest:** The authors declare no conflict of interest.

## Nomenclature

| | |
|---|---|
| $A$ | Cross-sectional area of the cut ($mm^2$) |
| $B$, $C$ | Constants in Equation (14) |
| $D$ | Cutter diameter (mm) |
| $v_c$ | Cutting speed (m/min) |
| $f_z$ | Feed rate (mm/z) |
| $a_p$ | Cutting depth (mm) |
| $a_e$ | Cutting width (mm) |
| $h$ | Uncut chip thickness (mm) |
| $h_c$ | Chip thickness (mm) |
| $h_{max}$ | Maximum uncut chip thickness (mm) |
| $R_c$ | Chip compression ratio |
| $\delta$ | Immersion angle at maximum uncut chip Thickness (deg) |
| $\theta$ | Instantaneous angle of immersion (deg) |
| $\varphi$ | Shear angle (deg) |
| $\beta$ | Mean friction angle (deg) |
| $\gamma$ | Rank angle (deg) |
| $r_n$ | Cutting edge radius (mm) |
| $F_x$, $F_y$ | Cutting forces measured by force measuring platform |
| $F_c$ | Total force in the cutting direction (N) |
| $F_{cc}$ | Cutting force for chip formation (N) |
| $F_{cp}$ | Cutting force for ploughing (N) |
| $F_t$ | Total force in thrust direction (N) |
| $F_{tc}$ | Thrust force for chip formation (N) |
| $F_{tp}$ | Thrust force for ploughing (N) |
| $F_s$ | Shear force on the shear plane (N) |
| $F_n$ | Normal force on the shear plane (N) |
| $F_u$ | Friction force on the rank face (N) |
| $F_v$ | Normal force on the rank face (N) |
| $l$ | Active cutting edge length (mm) |
| $\tau_s$ | Shear stress of MMCs (MPa) |
| $\tau_m$ | Shear stress of matrix material (MPa) |

## References


1. Rana, R.S.; Purohit, R.; Das, S. Review of recent studies in Al matrix composites. *Int. J. Sci. Eng. Res.* **2012**, *3*, 1–16.
2. Das, D.K.; Mishra, P.C.; Singh, S.; Thakur, R.K. Tool wear in turning ceramic reinforced aluminum matrix composites—A review. *J. Compos. Mater.* **2015**, *49*, 2949–2961.
3. El-Gallab, M.; Sklad, M. Machining of Al/SiC particulate metal-matrix composites: Part I: Tool performance. *J. Mater. Process. Technol.* **1998**, *83*, 151–158. [CrossRef]
4. Lin, J.T.; Bhattacharyya, D.; Lane, C. Machinability of a silicon-carbide reinforced aluminum metal-matrix composite. *Wear* **1995**, *181*, 883–888. [CrossRef]
5. Przestacki, D. Conventional and laser assisted machining of composite A359/20SiCp. *Procedia CIRP* **2014**, *14*, 229–233. [CrossRef]
6. Przestacki, D.; Jankowiak, M. Surface roughness analysis after laser assisted machining of hard to cut materials. *J. Phys. Conf. Ser.* **2014**, *483*, 012019. [CrossRef]
7. Przestacki, D.; Szymanski, P.; Wojciechowski, S. Formation of surface layer in metal matrix composite A359/20SiCP during laser assisted turning. *Compos. Part A Appl. Sci. Manuf.* **2016**, *91*, 370–379. [CrossRef]
8. Jenarthanan, M.; Prakash, A.R.; Jeyapaul, R. Modeling and analysis of process parameters on metal removal rate (MRR) in machining of aluminium titanium diboride (Al-$TiB_2$) composite. *Multidiscip. Model. Mater. Struct.* **2015**, *11*, 372–385. [CrossRef]

9. Krishnamurthy, K.; Venkatesh, J. Study on machining parameters of $TiB_2$ reinforced aluminum 6063 composites. *Int. J. Sci. Res. Publ.* **2013**, *3*, 130–137.
10. Mahamani, A. Machinability study of Al-5Cu-$TiB_2$ in-situ metal matrix composites fabricated by flux-assisted synthesis. *J. Miner. Mater. Charact. Eng.* **2011**, *10*, 1243–1254.
11. Anandakrishnan, V.; Mahamani, A. Investigations of flank wear, cutting force, and surface roughness in the machining of Al-6061-$TiB_2$ in situ metal matrix composites produced by flux-assisted synthesis. *Int. J. Adv. Manuf. Technol.* **2011**, *55*, 65–73. [CrossRef]
12. Xiong, Y.F.; Wang, W.H.; Jiang, R.S.; Lin, K.Y.; Song, G.D. Tool wear mechanisms for milling in situ $TiB_2$ particle-reinforced Al matrix composites. *Int. J. Adv. Manuf. Technol.* **2016**, *86*, 3517–3526. [CrossRef]
13. Xiong, Y.F.; Wang, W.H.; Jiang, R.S.; Lin, K.Y.; Song, G.D. Surface integrity of milling in-situ $TiB_2$ particle reinforced Al matrix composites. *Int. J. Refract. Met. Hard Mater.* **2016**, *54*, 407–416. [CrossRef]
14. Jiang, R.S.; Wang, W.H.; Song, G.D.; Wang, Z.Q. Experimental investigation on machinability of in situ formed $TiB_2$ particles reinforced Al MMCs. *J. Manuf. Process.* **2016**, *23*, 249–257.
15. Ge, Y.F.; Xu, J.H.; Yang, H.; Luo, S.B.; Fu, Y.C. Workpiece surface quality when ultra-precision turning of SiCp/Al composites. *J. Mater. Process. Technol.* **2008**, *203*, 166–175. [CrossRef]
16. Reddy, N.S.K.; Kwang-Sup, S.; Yang, M. Experimental study of surface integrity during end milling of Al/SiC particulate metal-matrix composites. *J. Mater. Process. Technol.* **2008**, *201*, 574–579. [CrossRef]
17. Wang, T.; Xie, L.J.; Wang, X.B.; Jiao, L.; Shen, J.W.; Xu, H.; Nie, F.M. Surface integrity of high speed milling of Al/SiC/65p aluminum matrix composites. *Procedia CIRP* **2013**, *8*, 475–480. [CrossRef]
18. Kishawy, H.A.; Kannan, S.; Balazinski, M. An energy based analytical force model for orthogonal cutting of metal matrix composites. *CIRP Ann. Manuf. Technol.* **2004**, *53*, 91–94. [CrossRef]
19. Merchant, M.E. Mechanics of the metal cutting process. I. Orthogonal cutting and a type 2 chip. *J. Appl. Phys.* **1945**, *16*, 267–275. [CrossRef]
20. Pramanik, A.; Zhang, L.C.; Arsecularatne, J.A. Prediction of cutting forces in machining of metal matrix composites. *Int. J. Mach. Tools Manuf.* **2006**, *46*, 1795–1803. [CrossRef]
21. Davim, J.P.; Silva, J.; Baptista, A.M. Experimental cutting model of metal matrix composites (MMCs). *J. Mater. Process. Technol.* **2007**, *183*, 358–362. [CrossRef]
22. El-Gallab, M.; Sklad, M. Machining of Al/SiC particulate metal matrix composites: Part II: Workpiece surface integrity. *J. Mater. Process. Technol.* **1998**, *83*, 277–285. [CrossRef]
23. Hung, N.P.; Boey, F.Y.C.; Khor, K.A.; Phua, Y.S.; Lee, H.F. Machinability of aluminum alloys reinforced with silicon carbide particulates. *J. Mater. Process. Technol.* **1996**, *56*, 966–977. [CrossRef]
24. Yan, C.; Zhang, L.C. Single-point scratching of 6061 Al alloy reinforced by different ceramic particles. *Appl. Compos. Mater.* **1994**, *1*, 431–447. [CrossRef]
25. Dabade, U.A.; Dapkekar, D.; Joshi, S.S. Modeling of chip-tool interface friction to predict cutting forces in machining of Al/SiCp composites. *Int. J. Mach. Tools Manuf.* **2009**, *49*, 690–700. [CrossRef]
26. Sikder, S.; Kishawy, H.A. Analytical model for force prediction when machining metal matrix composite. *Int. J. Mech. Sci.* **2012**, *59*, 95–103. [CrossRef]
27. Wang, M.L.; Chen, Z.; Chen, D.; Wu, Y.; Li, X.F.; Ma, N.H.; Wang, H.W. The constitutive model and processing map for in-situ 5wt% TiB2 reinforced 7050 Al alloy matrix composite. *Key Eng. Mater.* **2014**, *575*, 11–19. [CrossRef]
28. Pramanik, A.; Zhang, L.C.; Arsecularatne, J.A. Machining of metal matrix composites: Effect of ceramic particles on residual stress, surface roughness and chip formation. *Int. J. Mach. Tools Manuf.* **2008**, *48*, 1613–1625. [CrossRef]
29. Dandekar, C.R.; Shin, Y.C. Modeling of machining of composite materials: A review. *Int. J. Mach. Tools Manuf.* **2012**, *57*, 102–121. [CrossRef]
30. Trent, E.M.; Wright, P.K. *Metal Cutting*, 4th ed.; Butterworth-Heinemann: Oxford, UK, 2000.
31. Waldorf, D.J. A simplified model for ploughing forces in turning. *J. Manuf. Process.* **2006**, *8*, 76–82. [CrossRef]


© 2017 by the authors. Licensee MDPI, Basel, Switzerland. This article is an open access article distributed under the terms and conditions of the Creative Commons Attribution (CC BY) license (http://creativecommons.org/licenses/by/4.0/).